Since January 2020 Elsevier has created a COVID-19 resource centre with free information in English and Mandarin on the novel coronavirus COVID-19. The COVID-19 resource centre is hosted on Elsevier Connect, the company's public news and information website.

Short Article

Cell Host & Microbe

SARS-CoV-2 Omicron sublineages show comparable cell entry but differential neutralization by therapeutic antibodies

Graphical abstract

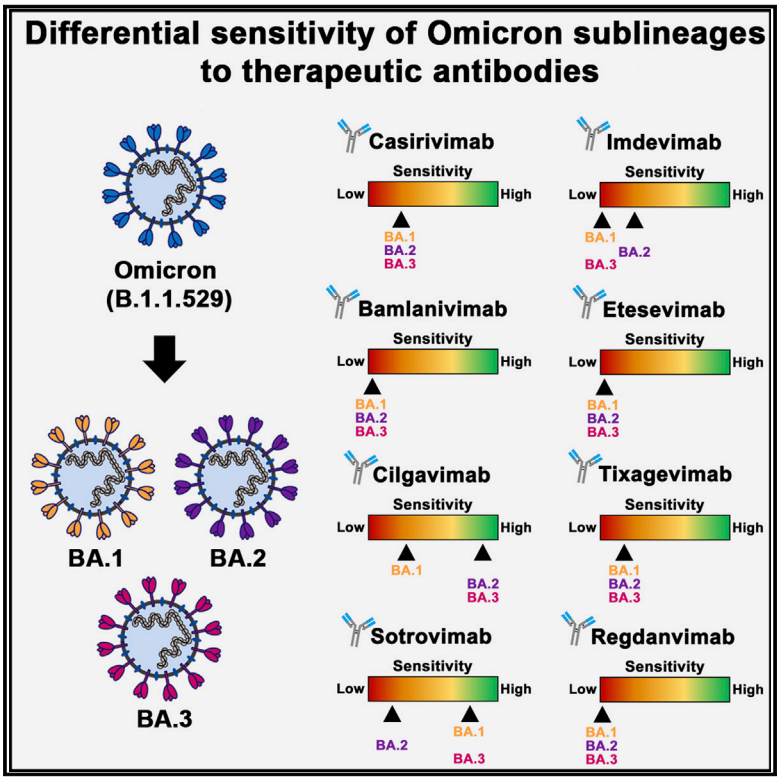

Highlights

- SARS-CoV-2 Omicron BA.1, BA.2, and BA.3 harbor shared and unique spike protein mutations
- BA.1, BA.2, and BA.3 enter and fuse target cells with similar efficiency
- mRNA vaccine boosters comparably increase neutralization of BA.1, BA.2, and BA.3
- BA.1, BA.2, and BA.3 differ regarding neutralization by therapeutic antibodies

Authors

Prerna Arora, Lu Zhang, Nadine Krüger, ..., Hans-Martin Jäck, Stefan Pöhlmann, Markus Hoffmann

Correspondence

spoehlmann@dpz.eu (S.P.), mhoffmann@dpz.eu (M.H.)

In brief

The SARS-CoV-2 Omicron variant contains at least three main sublineages that harbor shared and unique spike protein mutations. Arora et al. show that sublineages BA.1, BA.2, and BA.3 enter cells with similar efficiency and are comparably neutralized by antibodies induced by BNT162b2 booster vaccination but differ regarding neutralization by therapeutic antibodies.

Arora et al., 2022, Cell Host & Microbe *30*, 1103–1111
August 10, 2022
https://doi.org/10.1016/j.chom.2022.04.017

CellPress

Cell Host & Microbe

CellPress

Short Article

SARS-CoV-2 Omicron sublineages show comparable cell entry but differential neutralization by therapeutic antibodies

Prerna Arora,[1,2,7] Lu Zhang,[1,2,7] Nadine Krüger,[1,7] Cheila Rocha,[1,2] Anzhalika Sidarovich,[1,2] Sebastian Schulz,[3] Amy Kempf,[1,2] Luise Graichen,[1,2] Anna-Sophie Moldenhauer,[1] Anne Cossmann,[4] Alexandra Dopfer-Jablonka,[4,5,6] Georg M.N. Behrens,[4,5,6] Hans-Martin Jäck,[3] Stefan Pöhlmann,[1,2,8,*] and Markus Hoffmann[1,2,*]

[1]Infection Biology Unit, German Primate Center, Kellnerweg 4, 37077 Göttingen, Germany

[2]Faculty of Biology and Psychology, Georg-August-University Göttingen, Wilhelmsplatz 1, 37073 Göttingen, Germany

[3]Division of Molecular Immunology, Department of Internal Medicine 3, Friedrich-Alexander University of Erlangen-Nürnberg, Glückstraße 6, 91054 Erlangen, Germany

[4]Department for Rheumatology and Immunology, Hannover Medical School, Carl-Neuberg-Straße 1, 30625 Hannover, Germany

[5]German Centre for Infection Research (DZIF), partner site Hannover-Braunschweig, Inhoffenstraße 7, 38124 Braunschweig, Germany

[6]Centre for Individualised Infection Medicine (CiiM), Feodor-Lynen-Straße 7, 30625 Hannover, Germany

[7]These authors contributed equally

[8]Lead contact

*Correspondence: spoehlmann@dpz.eu (S.P.), mhoffmann@dpz.eu (M.H.)

https://doi.org/10.1016/j.chom.2022.04.017

SUMMARY

The Omicron variant of SARS-CoV-2 evades antibody-mediated neutralization with unprecedented efficiency. At least three Omicron sublineages have been identified—BA.1, BA.2, and BA.3—and BA.2 exhibits increased transmissibility. However, it is currently unknown whether BA.2 differs from the other sublineages regarding cell entry and antibody-mediated inhibition. Here, we show that BA.1, BA.2, and BA.3 enter and fuse target cells with similar efficiency and in an ACE2-dependent manner. However, BA.2 was not efficiently neutralized by seven of eight antibodies used for COVID-19 therapy, including Sotrovimab, which robustly neutralized BA.1. In contrast, BA.2 and BA.3 (but not BA.1) were appreciably neutralized by Cilgavimab, which could constitute a treatment option. Finally, all sublineages were comparably and efficiently neutralized by antibodies induced by BNT162b2 booster vaccination after previous two-dose homologous or heterologous vaccination. Collectively, the Omicron sublineages show comparable cell entry and neutralization by vaccine-induced antibodies but differ in susceptibility to therapeutic antibodies.

INTRODUCTION

The Omicron variant of SARS-CoV-2 was first detected in South Africa, Botswana, and Hong Kong in November 2021 and subsequently spread globally, rapidly outcompeting the previously dominating Delta variant (Jung et al., 2022; Karim and Karim, 2021). The viral spike (S) protein is the key target of the neutralizing antibody response, which critically contributes to SARS-CoV-2 control in convalescent and vaccinated individuals (Krammer, 2021; Lumley et al., 2021). The Omicron variant harbors more than 25 mutations in the S protein, and these allow for higher evasion from neutralizing antibodies than other variants of concern (VOCs) (Carreno et al., 2022; Dejnirattisai et al., 2022; Garcia-Beltran et al., 2022; Hoffmann et al., 2022; Rossler et al., 2022; Schmidt et al., 2022; VanBlargan et al., 2022; Zhang et al., 2022). In keeping with these findings, the Omicron variant efficiently spreads in populations with preexisting SARS-CoV-2 immunity (Altarawneh et al., 2022; Collie et al., 2022; Lyngse et al., 2022).

At least three Omicron sublineages are known: BA.1, BA.2, and BA.3 (Mahase, 2022). In addition, a BA.1 sublineage harboring mutation R346K in the S protein (BA.1.1) has been observed (Mahase, 2022). The sublineages display remarkable differences in the amino acid sequence of their S proteins, particularly with respect to the N-terminal domain (NTD) and the receptor-binding domain (RBD; the portion of the S protein that binds to the ACE2 receptor; Hoffmann et al., 2020; Zhou et al., 2020), which both are known to harbor key epitopes of neutralizing antibodies (McCallum et al., 2021; Piccoli et al., 2020). In general, BA.1 and BA.3 seem to be much more closely related to each other than to BA.2 on the basis of their S protein mutations.

In several countries, including Denmark and the United Kingdom (Lyngse et al., 2022; Mahase, 2022), BA.2 is currently becoming dominant, driving a new wave of infections. It has been suggested that BA.2 might have a fitness advantage, i.e., might exhibit higher transmissibility than the other Omicron sublineages (Cheng et al., 2022; Lyngse et al., 2022). However, it is at present unclear whether altered host cell interactions during viral

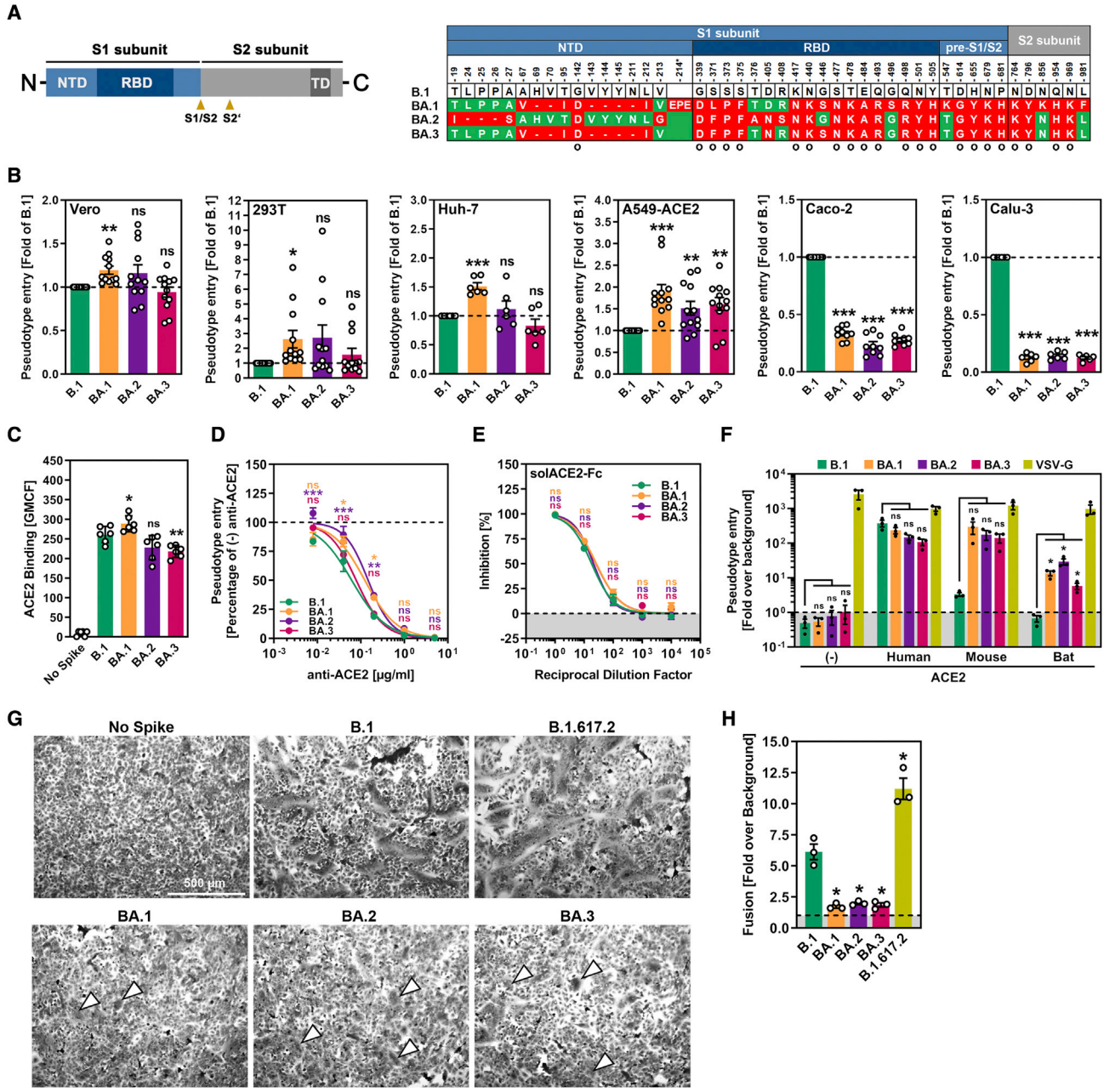

Figure 1. S proteins of Omicron sublineages do not exhibit major differences in ACE2 usage or ability to drive cell-cell and virus-cell fusion

(A) Schematic overview of the SARS-CoV-2 spike (S) protein domain structure (left) and summary of the mutations found in the different Omicron sublineages (right; numbering is according to the S protein of SARS-CoV-2 B.1). S protein residues that are identical between the S proteins of some Omicron sublineages and B.1 are marked in green, whereas mutated residues are highlighted in red (note: the BA.1 S protein harbors an insertion between amino acid residues 214 and 215). Further, mutations found in all Omicron sublineages are indicated by a circle. Abbreviations: NTD, N-terminal domain; RBD, receptor-binding domain; TD, transmembrane domain; S1/S2 and S2', cleavage sites in the S protein.

(B) S-protein-driven cell entry. We added particles bearing the indicated S proteins (or no S protein) to the indicated cell lines and analyzed cell entry by measuring the activity of virus-encoded firefly luciferase in cell lysates 16–18 h after inoculation. Presented are the average (mean) data from 6–12 biological replicates (each conducted with four technical replicates) in which cell entry was normalized against B.1 (set as 1). Error bars show the SEM. Statistical significance was assessed by two-tailed Student's t tests ($p > 0.05$, not significant [ns]; $p \leq 0.05$, *; $p \leq 0.01$, **; $p \leq 0.001$, ***). Please also see Figure S1.

(C) ACE2 binding efficiency. 293T cells transiently expressing the indicated S proteins (or no S protein) where first incubated with soluble ACE2 fused to the Fc portion of human immunoglobulin G (solACE2-Fc) and subsequently incubated with an Fc-specific AlexaFluor-488-coupled secondary antibody; then, solACE2-Fc binding was analyzed by flow cytometry. Presented are the average (mean) data from six biological replicates (each conducted with single samples) in which ACE2 binding was normalized against B.1 (set as 1). Error bars show the SEM. Statistical significance was assessed by two-tailed Student's t tests ($p > 0.05$, not significant [ns]; $p \leq 0.05$, *; $p \leq 0.01$, **).

(legend continued on next page)

entry into target cells contribute to the increased transmissibility of BA.2. Furthermore, it is incompletely understood whether BA.2 differs from the other Omicron sublineages regarding susceptibility to neutralization by therapeutic antibodies, which are instrumental to COVID-19 treatment, and antibodies produced upon vaccination. Here, we compared BA.1, BA.2, and BA.3 for host cell entry and sensitivity to neutralization by therapeutic and vaccine-induced antibodies.

RESULTS

The S proteins of the Omicron sublineages differ in their NTD and RBD sequences

Relative to the S protein of the ancestral B.1 virus, the S proteins of the BA.1, BA.2, and BA.3 sublineages harbor more than 25 mutations. However, there are also substantial sequence differences between the Omicron sublineages (Figure 1A). For instance, residues 24–26 are missing from the NTD of the BA.2 S protein but are present in the S proteins of BA.1 and BA.3 (Figure 1A). Conversely, residues 69–70 and 143–145 are absent from the S proteins of BA.1 and BA.3 but are present in the S protein of BA.2 (Figure 1A). Finally, each sublineage harbors unique mutations, but it is currently unclear whether the sublineages differ in host cell entry and antibody-mediated neutralization.

Comparable cell tropism of Omicron sublineages

We addressed cell entry of the Omicron sublineages and its inhibition by using rhabdoviral pseudotype particles (pp) harboring SARS-CoV-2 S proteins, which faithfully mimic SARS-CoV-2 entry and its blockade by neutralizing antibodies (Hoffmann et al., 2021a; Riepler et al., 2020). We first analyzed whether the Omicron sublineages differ in their capacity to enter cell lines frequently used for SARS-CoV-2 research. Particles bearing the S proteins of BA.1, BA.2, or BA.3 entered A549-ACE2 (human lung) cells with higher efficiency than particles bearing the B.1 S protein ($B.1_{pp}$) (Figure 1B). Particles bearing the BA.1 S protein also entered Vero (African green monkey kidney), 293T (human kidney), and Huh-7 (human liver) with slightly higher efficiency than $B.1_{pp}$, whereas such differences were not observed for $BA.2_{pp}$ or $BA.3_{pp}$. In contrast, entry of $BA.1_{pp}$, $BA.2_{pp}$, and $BA.3_{pp}$ into Caco-2 (human colon) and Calu-3 (human lung) was less efficient than that of $B.1_{pp}$ (Figure 1B), and this phenotype most likely reflects differences in the choice of the S-protein-activating host cell proteases (Hui et al., 2022; Meng et al., 2022). In sum, our analysis reveals no marked differences in host cell entry of BA.1, BA.2, and BA.3, although BA.1 might enter certain cell lines with slightly increased efficiency.

Omicron sublineages efficiently bind ACE2 and enter cells in an ACE2-dependent fashion

We next assessed whether comparable host cell entry is associated with comparable ACE2 binding. Indeed, 293T cells expressing the S proteins of B.1 or the Omicron sublineages bound to soluble ACE2 with roughly comparable efficiency, although ACE2 binding of the BA.3 S protein was slightly reduced (Figure 1C). In keeping with these findings, an anti-ACE2 antibody and soluble ACE2 blocked host cell entry of $B.1_{pp}$, $BA.1_{pp}$, $BA.2_{pp}$, and $BA.3_{pp}$ with roughly comparable efficiency (Figures 1D and E), although $BA.3_{pp}$ was slightly more sensitive to inhibition by the anti-ACE2 antibody than $BA.1_{pp}$ and $BA.2_{pp}$. Finally, all particles efficiently used human, mouse, and horseshoe bat ACE2 for entry; the only exception was $B.1_{pp}$, which failed to use mouse and bat ACE2 for efficient entry (Figure 1F), in keeping with published findings (Hoffmann et al., 2022).

Reduced cell-cell fusion by all Omicron sublineages

The S-protein-mediated fusion of infected with uninfected cells results in the formation of syncytia, which are believed to contribute to COVID-19 pathogenesis (Bussani et al., 2020; Xu et al., 2020). The ability of the BA.1 S protein to drive cell-cell fusion and syncytia formation was previously found to be reduced, whereas the S protein of the Delta variant (B.1.617.2) was reported to exhibit increased capacity to mediate cell-cell fusion (Arora et al., 2021; Meng et al., 2022; Saito et al., 2022; Suzuki et al., 2022; Zhao et al., 2022). Employing qualitative (microscopic) and quantitative (beta-galactosidase reporter protein

(D) Blockade of S-protein-driven cell entry by an anti-ACE2 antibody. Vero cells were preincubated with serial dilutions of anti-ACE2 antibody before particles bearing the indicated S proteins were added. S-protein-driven cell entry was analyzed and normalized to samples without anti-ACE2 antibody (set as 1). Presented are the average (mean) data of three biological replicates, each performed with four technical replicates. Error bars show the SEM. Statistical significance was assessed by two-way analysis of variance with Dunnett's post hoc tests ($p > 0.05$, not significant [ns]; $p \leq 0.05$, *; $p \leq 0.01$, **; $p \leq 0.001$, ***). Please also see Tables S1 and S2.

(E) Blockade of S-protein-driven cell entry by solACE2-Fc. Particles bearing the indicated S proteins were preincubated with serial dilutions of solACE2-Fc (or no solACE2-Fc) before being added to Vero cells. S-protein-driven cell entry was analyzed and normalized to samples without solACE2-Fc (= 0% inhibition). Presented are the average (mean) data of three biological replicates, each performed with four technical replicates. Error bars show the SEM. Statistical significance was assessed by two-way analysis of variance with Dunnett's post hoc tests ($p > 0.05$, not significant [ns]) .

(F) Usage of mouse and bat ACE2 by Omicron S proteins. BHK-21 cells transiently expressing human, mouse, or horseshoe bat (*Rhinolophus pearsonii*) ACE2 orthologs (or no ACE2) were inoculated with particles bearing the indicated S proteins or VSV glycoprotein (VSV-G). Cell entry of pseudovirus particles was analyzed and normalized to particles bearing no viral glycoprotein (set as 1; indicated by dashed line). Presented are the average (mean) data of three biological replicates, each performed with four technical replicates. Error bars show the SEM. Statistical significance was assessed by two-tailed Student's t tests ($p > 0.05$, not significant [ns]; $p \leq 0.05$, *).

(G) Qualitative fusion assay. A549-ACE2 cells transfected to express the indicated S proteins (or no S protein) were fixed 24 h after transfection and stained with May-Gruenwald and Giemsa solution before microscopic images were taken (scale bar, 500 μm). Arrowheads indicate small syncytia in cells expressing the S proteins of the different Omicron sublineages.

(H) Quantitative fusion assay. 24 h after transfection, 293T cells transiently expressing the indicated S proteins (or no S protein) along with the beta-galactosidase alpha fragment were resuspended and seeded on top of A549-ACE2 cells transiently expressing the beta-galactosidase omega fragment. After an additional 24 h of incubation, beta-galactosidase substrate was added, and luminescence was recorded. Presented are the average (mean) data of three biological replicates, each performed with four technical replicates. Error bars show the SEM. Statistical significance was assessed by two-tailed Student's t tests ($p \leq 0.05$, *).

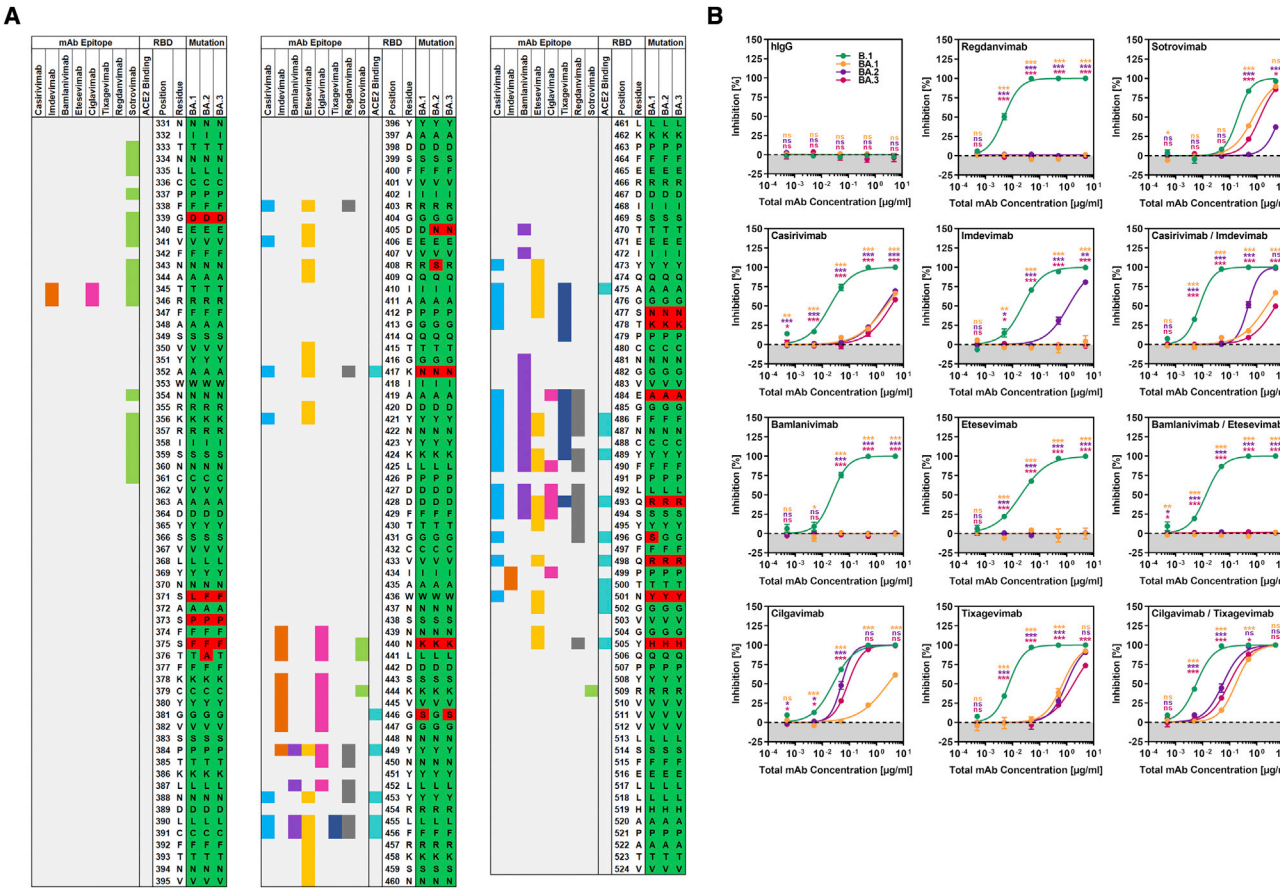

Figure 2. S proteins of Omicron sublineages differ in terms of their resistance to therapeutic antibodies

(A) Schematic overview of the SARS-CoV-2 S protein RBD (numbering is according to the S protein of SARS-CoV-2 B.1). Mutations found in the RBDs of the Omicron sublineages (compared with the B.1 S protein) are highlighted in red, whereas identical amino acid residues are marked in green. RBD residues that make direct contact with ACE2 or that are recognized as epitopes for therapeutic antibodies are highlighted.

(B) Particles bearing the indicated S proteins were preincubated with serial dilutions of individual monoclonal antibodies used for COVID-19 treatment or cocktails thereof or an irrelevant control antibody (hIgG) before being added to Vero cells. Of note, for antibody cocktails, we used each antibody at half concentration in order to keep total antibody concentrations constant. S-protein-driven cell entry was analyzed and normalized to samples without antibody (= 0% inhibition). Presented are the average (mean) data of three biological replicates, each performed with four technical replicates. Error bars show the SEM. Statistical significance was assessed by two-way analysis of variance with Dunnett's post hoc tests ($p > 0.05$, not significant [ns]; $p \leq 0.05$, *; $p \leq 0.01$, **; $p \leq 0.001$, ***). Please see also Tables S1 and S2.

reconstitution) cell-to-cell fusion assays, we confirmed that syncytium formation by the BA.1 S protein is less efficient than that of the B.1 S protein, whereas the B.1.617.2 S protein is more adept at syncytium formation (Figures 1G and 1H). Further, no difference in syncytium formation was observed between the Omicron sublineages, indicating that the mutations in the respective S proteins do not alter the ability to fuse cells (Figures 1G and 1H).

Differential sensitivity of Omicron sublineages to neutralization by therapeutic monoclonal antibodies

Recombinant monoclonal antibodies that bind to the S protein and neutralize SARS-CoV-2 are successfully employed for COVID-19 therapy. Therefore, we analyzed whether the Omicron sublineages differ in sensitivity to neutralization by such therapeutic antibodies. Unspecific immunoglobulin did not interfere with particle entry, whereas all therapeutic antibodies efficiently neutralized $B.1_{pp}$, as expected (Figures 2A and 2B). In contrast, most antibodies failed to neutralize the Omicron sublineages or neutralized with markedly less efficiency than $B.1_{pp}$, in keeping with the mutations' being located in the epitopes of these antibodies (Figures 2A and 2B) (Dong et al., 2021; Hansen et al., 2020; Jones et al., 2021; Kim et al., 2021; Pinto et al., 2020; Shi et al., 2020). Further, differences in neutralization of the sublineages by the remaining antibodies were noted. Thus, $BA.1_{pp}$ were only appreciably neutralized by sotrovimab, and neutralization was not as efficient as that measured for $B.1_{pp}$ (Figure 2B), potentially as a result of mutations G339D and N440K in the BA.1 S protein (Figure 2A). In contrast, $BA.2_{pp}$ were robustly neutralized only by cilgavimab, and neutralization efficiency was lower than that detected for $B.1_{pp}$ (Figure 2B); this effect might result from mutations N440K, E484A, and Q493R in the BA.2 S protein (Figure 2A). Further, $BA.3_{pp}$ were neutralized by cilgavimab and sotrovimab although not with the same efficiency

as $B.1_{pp}$ (Figure 2B), probably as a result of mutations G339D, N440K, G446S, E484A, and Q493R in BA.3 S protein (Figure 2A). Finally, compared with the most active single antibodies, combinations of casirivimab and imdevimab, bamlanivimab and etesevimab, or cilgavimab and tixagevimab did not improve neutralization (Figure 2B). Collectively, none of the antibodies tested neutralized particles bearing BA.1, BA.2, or BA.3 S protein with maximal efficiency, and sotrovimab is not likely to be very effective in patients infected with sublineage BA.2.

Comparable neutralization of the Omicron sublineages by antibodies induced upon BNT162b2 booster vaccination after primary two-dose homologous or heterologous vaccination with BNT162b2 and/or ChAdOx1-S vaccines

We previously reported that BA.1 is highly resistant to antibodies induced upon SARS-CoV-2 infection or double vaccination with the mRNA-based vaccine BNT162b2 (BNT) (Hoffmann et al., 2022). In contrast, antibodies induced by three vaccinations appreciably neutralized BA.1, and triple vaccination has been reported to provide robust protection against severe disease and death upon infection with the Omicron variant (Abu-Raddad et al., 2022; Accorsi et al., 2022). Further, improved neutralization was also measured for antibodies induced upon heterologous vaccination with BNT162b2 and the Astra Zeneca (AZ) vaccine ChAdOx1-S (Hoffmann et al., 2021b). However, it was unclear whether this protection extended to all Omicron sublineages. We addressed this question by analyzing sera from 15 donors after triple BNT162b2 (BNT/BNT/BNT) vaccination and heterologous AZ/BNT/BNT or AZ/AZ/BNT vaccination. Neutralization of $B.1_{pp}$ was robust, and neutralization of particles bearing the S proteins of the Omicron sublineages was roughly 4- to 6-fold reduced such that there were no significant differences between the sublineages (Figure 3A) and similar results were obtained for sera from individuals vaccinated with AZ/BNT/BNT (Figure 3B) and AZ/AZ/BNT (Figure 3C). These results indicate that homologous BNT or heterologous BNT/AZ triple vaccination should provide comparable protection against all Omicron sublineages.

DISCUSSION

Our results suggest that increased transmissibility of BA.2 is not due to increased ACE2 binding, cell-cell fusion, or virus-cell entry and that the therapeutic antibody cilgavimab (but not sotrovimab) can be employed for treatment of BA.2-infected COVID-19 patients.

Previous studies noted that BA.1 and BA.2 cases do not differ appreciably with regard to age, sex, hospitalization, or mortality (Fonager et al., 2022). However, differences in transmissibility were noted. Thus, BA.2 was associated with a higher secondary attack rate than BA.1 in a study of Danish households (Lyngse et al., 2022). Specifically, household members were more susceptible to BA.2 than to BA.1 infection, and this effect was more pronounced for vaccinated than for unvaccinated individuals. Further, transmission of BA.2 by unvaccinated individuals was higher than that of BA.1, but this difference was not seen for vaccinated individuals (Lyngse et al., 2022). Thus, apart from immune evasion, BA.2 seems to exhibit higher inherent transmissibility than BA.1. The present study suggests that the increased transmissibility of BA.2 is not due to increased ACE2 binding of the BA.2 S protein or more efficient S-protein-driven cell-cell and virus-cell fusion. In the light of these findings, one can speculate that BA.2 might differ from BA.1 with regard to the usage of attachment factors that might promote spread in the upper respiratory tract, potentially heparan sulfate proteoglycans (Clausen et al., 2020). Alternatively, BA.2 might be better adapted to the temperatures in the upper respiratory tract than BA.1, or BA.2 virions might be more stable.

Recombinant monoclonal antibodies that bind to the SARS-CoV-2 S protein and neutralize the virus can markedly reduce the risk of serve disease and death when applied early after SARS-CoV-2 infection (Weinreich et al., 2021). Several such antibodies have obtained emergency use authorization for COVID-19 treatment, but their effectiveness can be compromised by resistance-conferring mutations in the S protein. In fact, initial studies conducted with the S proteins of BA.1 reported resistance against most antibodies (Carreno et al., 2022; Dejnirattisai et al., 2022; Garcia-Beltran et al., 2022; Hoffmann et al., 2022; Rossler et al., 2022; Schmidt et al., 2022; VanBlargan et al., 2022; Zhang et al., 2022), although sotrovimab constituted a notable exception. However, the present study revealed important differences between the Omicron sublineages in terms of susceptibility to neutralization by sotrovimab and other antibodies. Neutralization of BA.1 and BA.3 by sotrovimab was only slightly less efficient than that of B.1, whereas neutralization of BA.2 was inefficient. Further, cilgavimab neutralized BA.2 and BA.3 with appreciable efficiency but was poorly active against BA.1. Our findings, which are in keeping with recent reports (Bruel et al., 2022; Iketani et al., 2022; Takashita et al., 2022), indicate that different antibodies should be chosen for treatment of COVID-19 patients infected with different Omicron sublineages, and sotrovimab and cilgavimab constitute important treatment options.

Vaccination is the major tool for combatting the pandemic, and three immunizations with mRNA-based vaccines have been shown to robustly protect against severe disease and death from infection by the Omicron variant (Abu-Raddad et al., 2022). However, it is largely unclear whether the neutralizing antibody response induced upon triple vaccination will comparably inhibit all Omicron sublineages. The present study suggests that this will be the case: all Omicron sublineages were robustly and comparably neutralized by antibodies induced upon BNT162b2 booster vaccination of individuals who had previously received two-dose homologous or heterologous vaccinations with BNT162b2 and/or ChAdOx1-S, although neutralization was less efficient than that measured for $B.1_{pp}$, in keeping with expectations (Hoffmann et al., 2022). Collectively, these data indicate that individuals who received booster shots of BNT162b2 are likely to be comparably protected against severe disease induced by Omicron sublineages BA.1, BA.2, and BA.3, in keeping with recent studies showing comparable neutralization of BA.1 and BA.2 by antibodies induced upon double and triple vaccination with BNT162b2 (Arora et al., 2022; Iketani et al., 2022; Yu et al., 2022).

Limitations of the study

We present, to our knowledge, the first side-by-side analysis of the Omicron sublineages BA.1, BA.2, and BA.3 for host cell entry

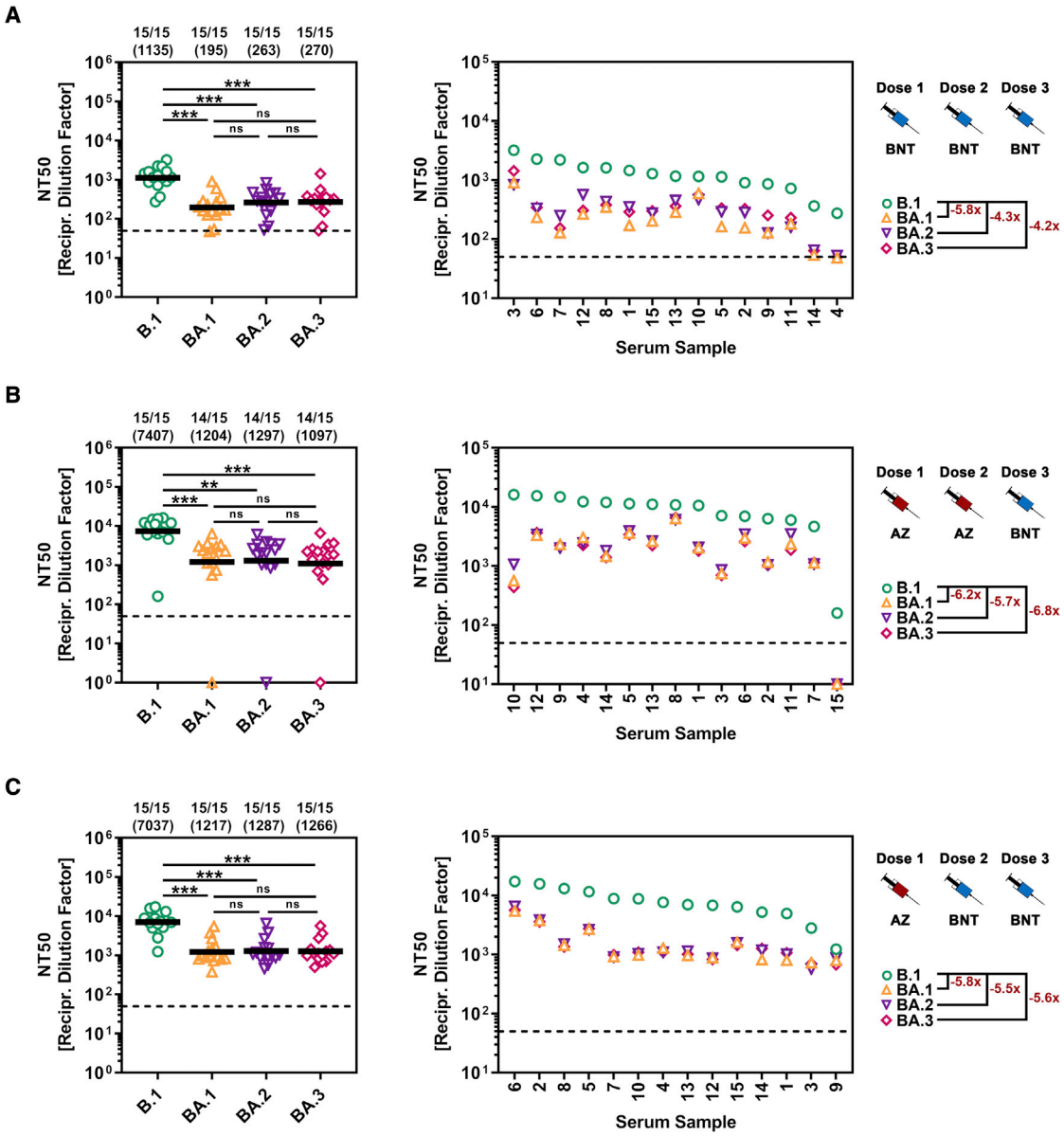

Figure 3. S proteins of Omicron sublineages do not differ in sensitivity to neutralization by antibodies elicited upon triple vaccination with BNT162b2 or BNT162b2/ChAdOx1-S

(A) Left: particles bearing the indicated S proteins were preincubated with serial dilutions of serum from individuals vaccinated three times with BNT162b2 (BNT) before being added to Vero cells. S-protein-driven cell entry was analyzed and used for calculating the neutralizing titer 50 (NT50). Presented are the combined data for 15 sera (black lines show the geometric mean; the dashed line indicates the lowest serum dilution tested). Numerical values above the graph indicate the proportion of sera with reactivity against the respective S-protein-bearing particles and the geometric mean NT50. The statistical significance of differences between individual groups was assessed by two-tailed Mann-Whitney test ($p > 0.05$, not significant [ns]; $p \leq 0.05$, *; $p \leq 0.01$, **; $p \leq 0.001$, ***). Right: individual NT50 values per serum (ranked according to neutralizing activity against B.1) and fold change in neutralizing activity compared with that of B.1. Please also see Figure S2 and Table S3.

(B) The experiment was performed as described for (A), but this time 15 sera from individuals who had been vaccinated twice with ChAdOx1-S (AZ) and then once with BNT162b2 (BNT) were analyzed. Please also see Figure S2 and Table S3.

(C) The experiment was performed as described for (A), but this time 15 sera from individuals who had been vaccinated once with ChAdOx1-S (AZ) and then twice with BNT162b2 (BNT) were analyzed. Please also see Figure S2 and Table S3.

and antibody-mediated neutralization, and our findings are of immediate interest to clinical practice. However, the following limitations of our study should be noted. We worked with pseudotype particles, and results await confirmation with authentic SARS-CoV-2. Further, we studied cell lines that might not fully reflect primary viral target cells. We also observed comparable neutralization of the Omicron sublineages by sera from individuals who had received booster shots of BNT162b2 after previous

CellPress

BNT/BNT, AZ/AZ, or AZ/BNT vaccination but cannot rule out that different vaccines or vaccination regimens might result in differential inhibition of the Omicron sublineages. Finally, determining the relative decrease in neutralization of the Omicron sublineages over time will require a longitudinal analysis.

STAR★METHODS

Detailed methods are provided in the online version of this paper and include the following:

- KEY RESOURCES TABLE
- RESOURCE AVAILABILITY
  - Lead contact
  - Materials availability
  - Data and code availability
- EXPERIMENTAL MODEL AND SUBJECT DETAILS
  - Cell cultures
  - Human subjects
- METHODS DETAILS
  - Plasmids
  - Production of soluble ACE2
  - Production of pseudotyped particles
  - Analysis of S-protein-mediated cell entry
  - Analysis of ACE2 binding by flow cytometry
  - Qualitative cell-to-cell fusion assay
  - Quantitative cell-to-cell fusion assay
- QUANTIFICATION AND STATISTICAL ANALYSIS

SUPPLEMENTAL INFORMATION

Supplemental information can be found online at https://doi.org/10.1016/j.chom.2022.04.017.

ACKNOWLEDGMENTS

We thank B.J. Bosch, R. Cattaneo, G. Herrler, A. Maisner, S. Ludwig, T. Pietschmann, and G. Zimmer for providing reagents. We gratefully acknowledge the originating laboratories responsible for obtaining the specimens, as well as the submitting laboratories where the genome data were generated and shared via GISAID, on which this research is based. S.P. acknowledges funding by the BMBF (01KI2006D, 01KI20328A, and 01KX2021), Ministry for Science and Culture of Lower Saxony (14-76103-184 and MWK HZI COVID-19), and German Research Foundation (DFG; PO 716/11-1 and PO 716/14-1). N.K. received funding from the BMBF (01KI2074A). H.-M.J. received funding from the BMBF (01KI2043; NaFoUniMedCovid19-COVIM: 01KX2021), Bavarian State Ministry for Science and the Arts, and DFG through the research training groups RTG1660 and TRR130. G.M.N.B. acknowledges funding by the German Center for Infection Research (80018019238) and European Regional Development Fund (Defeat Corona, ZW7-8515131, together with A.D.-J.).

AUTHOR CONTRIBUTIONS

Conceptualization, P.A., S.P., and M.H.; funding acquisition, N.K., H.M.J., G.M.N.B., and S.P.; investigation, P.A., L.Z., N.K., C.R., A.S., A.K., L.G., A.-S.M., and M.H.; essential resources, S.S., A.C., A.D.-J., G.M.N.B., and H.-M.J.; writing, S.P. and M.H.; review and editing, all authors.

DECLARATION OF INTERESTS

The authors declare no competing interests.

Received: March 17, 2022
Revised: April 20, 2022
Accepted: April 29, 2022
Published: May 6, 2022

REFERENCES

Abu-Raddad, L.J., Chemaitelly, H., Ayoub, H.H., AlMukdad, S., Yassine, H.M., Al-Khatib, H.A., Smatti, M.K., Tang, P., Hasan, M.R., Coyle, P., et al. (2022). Effect of mRNA vaccine boosters against SARS-CoV-2 omicron infection in Qatar. N. Engl. J. Med. NEJMoa2200797. https://doi.org/10.1056/NEJMoa2200797.

Accorsi, E.K., Britton, A., Fleming-Dutra, K.E., Smith, Z.R., Shang, N., Derado, G., Miller, J., Schrag, S.J., and Verani, J.R. (2022). Association between 3 doses of mRNA COVID-19 vaccine and symptomatic infection caused by the SARS-CoV-2 omicron and Delta variants. JAMA *327*, 639–651. https://doi.org/10.1001/jama.2022.0470.

Altarawneh, H.N., Chemaitelly, H., Hasan, M.R., Ayoub, H.H., Qassim, S., AlMukdad, S., Coyle, P., Yassine, H.M., Al-Khatib, H.A., Benslimane, F.M., et al. (2022). Protection against the omicron variant from previous SARS-CoV-2 infection. N. Engl. J. Med. *386*, 1288–1290. https://doi.org/10.1056/NEJMc2200133.

Arora, P., Sidarovich, A., Kruger, N., Kempf, A., Nehlmeier, I., Graichen, L., Moldenhauer, A.S., Winkler, M.S., Schulz, S., Jack, H.M., et al. (2021). B.1.617.2 enters and fuses lung cells with increased efficiency and evades antibodies induced by infection and vaccination. Cell Rep. *37*, 109825. https://doi.org/10.1016/j.celrep.2021.109825.

Arora, P., Zhang, L., Rocha, C., Sidarovich, A., Kempf, A., Schulz, S., Cossmann, A., Manger, B., Baier, E., Tampe, B., et al. (2022). Comparable neutralisation evasion of SARS-CoV-2 omicron subvariants BA.1, BA.2, and BA.3. Lancet Infect. Dis. S1473-3099(22)00224-9. https://doi.org/10.1016/s1473-3099(22)00224-9(22)00224-9.

Berger Rentsch, M., and Zimmer, G. (2011). A vesicular stomatitis virus replicon-based bioassay for the rapid and sensitive determination of multi-species type I interferon. PLoS One *6*, e25858. https://doi.org/10.1371/journal.pone.0025858.

Brinkmann, C., Hoffmann, M., Lubke, A., Nehlmeier, I., Kramer-Kuhl, A., Winkler, M., and Pohlmann, S. (2017). The glycoprotein of vesicular stomatitis virus promotes release of virus-like particles from tetherin-positive cells. PLoS One *12*, e0189073. https://doi.org/10.1371/journal.pone.0189073.

Bruel, T., Hadjadj, J., Maes, P., Planas, D., Seve, A., Staropoli, I., Guivel-Benhassine, F., Porrot, F., Bolland, W.H., Nguyen, Y., et al. (2022). Serum neutralization of SARS-CoV-2 Omicron sublineages BA.1 and BA.2 in patients receiving monoclonal antibodies. Nat. Med. https://doi.org/10.1038/s41591-022-01792-5.

Burkard, C., Bloyet, L.-M., Wicht, O., van Kuppeveld, F.J., Rottier, P.J.M., de Haan, C.A.M., and Bosch, B.J. (2014). Dissecting virus entry: Replication-independent analysis of virus binding, internalization, and penetration using minimal complementation of β-galactosidase. PLoS One *9*, e101762. https://doi.org/10.1371/journal.pone.0101762.

Bussani, R., Schneider, E., Zentilin, L., Collesi, C., Ali, H., Braga, L., Volpe, M.C., Colliva, A., Zanconati, F., Berlot, G., et al. (2020). Persistence of viral RNA, pneumocyte syncytia and thrombosis are hallmarks of advanced COVID-19 pathology. EBioMedicine *61*, 103104. https://doi.org/10.1016/j.ebiom.2020.103104.

Carreno, J.M., Alshammary, H., Tcheou, J., Singh, G., Raskin, A.J., Kawabata, H., Sominsky, L.A., Clark, J.J., Adelsberg, D.C., Bielak, D.A., et al.; PSP-PARIS Study Group (2022). Activity of convalescent and vaccine serum against SARS-CoV-2 Omicron. Nature *602*, 682–688. https://doi.org/10.1038/s41586-022-04399-5.

Cheng, V.C.C., Ip, J.D., Chu, A.W.H., Tam, A.R., Chan, W.M., Abdullah, S.M.U., Chan, B.P.C., Wong, S.C., Kwan, M.Y.W., Chua, G.T., et al. (2022). Rapid spread of SARS-CoV-2 Omicron subvariant BA.2 in a single-source community outbreak. Clin. Infect. Dis. ciac203. https://doi.org/10.1093/cid/ciac203.

Clausen, T.M., Sandoval, D.R., Spliid, C.B., Pihl, J., Perrett, H.R., Painter, C.D., Narayanan, A., Majowicz, S.A., Kwong, E.M., McVicar, R.N., et al. (2020). SARS-CoV-2 infection depends on cellular heparan sulfate and ACE2. Cell *183*, 1043–1057.e15. https://doi.org/10.1016/j.cell.2020.09.033.

Collie, S., Champion, J., Moultrie, H., Bekker, L.G., and Gray, G. (2022). Effectiveness of BNT162b2 vaccine against omicron variant in South Africa. N. Engl. J. Med. *386*, 494–496. https://doi.org/10.1056/NEJMc2119270.

Dejnirattisai, W., Shaw, R.H., Supasa, P., Liu, C., Stuart, A.S., Pollard, A.J., Liu, X., Lambe, T., Crook, D., Stuart, D.I., et al. (2022). Reduced neutralisation of SARS-CoV-2 omicron B.1.1.529 variant by post-immunisation serum. Lancet *399*, 234–236. https://doi.org/10.1016/S0140-6736(21)02844-0.

Dong, J., Zost, S.J., Greaney, A.J., Starr, T.N., Dingens, A.S., Chen, E.C., Chen, R.E., Case, J.B., Sutton, R.E., Gilchuk, P., et al. (2021). Genetic and structural basis for SARS-CoV-2 variant neutralization by a two-antibody cocktail. Nat. Microbiol. *6*, 1233–1244. https://doi.org/10.1038/s41564-021-00972-2.

Fonager, J., Bennedbaek, M., Bager, P., Wohlfahrt, J., Ellegaard, K.M., Ingham, A.C., Edslev, S.M., Stegger, M., Sieber, R.N., Lassauniere, R., et al. (2022). Molecular epidemiology of the SARS-CoV-2 variant omicron BA.2 sub-lineage in Denmark, 29 november 2021 to 2 january 2022. Euro Surveill. *27*, 2200181. https://doi.org/10.2807/1560-7917.ES.2022.27.10.2200181.

Garcia-Beltran, W.F., St Denis, K.J., Hoelzemer, A., Lam, E.C., Nitido, A.D., Sheehan, M.L., Berrios, C., Ofoman, O., Chang, C.C., Hauser, B.M., et al. (2022). mRNA-based COVID-19 vaccine boosters induce neutralizing immunity against SARS-CoV-2 Omicron variant. Cell *185*, 457–466.e4. https://doi.org/10.1016/j.cell.2021.12.033.

Hansen, J., Baum, A., Pascal, K.E., Russo, V., Giordano, S., Wloga, E., Fulton, B.O., Yan, Y., Koon, K., Patel, K., et al. (2020). Studies in humanized mice and convalescent humans yield a SARS-CoV-2 antibody cocktail. Science *369*, 1010–1014. https://doi.org/10.1126/science.abd0827.

Hoffmann, M., Arora, P., Groß, R., Seidel, A., Hornich, B.F., Hahn, A.S., Kruger, N., Graichen, L., Hofmann-Winkler, H., Kempf, A., et al. (2021a). SARS-CoV-2 variants B.1.351 and P.1 escape from neutralizing antibodies. Cell *184*, 2384–2393.e12. https://doi.org/10.1016/j.cell.2021.03.036.

Hoffmann, M., Kleine-Weber, H., Schroeder, S., Kruger, N., Herrler, T., Erichsen, S., Schiergens, T.S., Herrler, G., Wu, N.H., Nitsche, A., et al. (2020). SARS-CoV-2 cell entry depends on ACE2 and TMPRSS2 and is blocked by a clinically proven protease inhibitor. Cell *181*, 271–280.e8. https://doi.org/10.1016/j.cell.2020.02.052.

Hoffmann, M., Kruger, N., Schulz, S., Cossmann, A., Rocha, C., Kempf, A., Nehlmeier, I., Graichen, L., Moldenhauer, A.S., Winkler, M.S., et al. (2022). The Omicron variant is highly resistant against antibody-mediated neutralization: implications for control of the COVID-19 pandemic. Cell *185*, 447–456.e11. https://doi.org/10.1016/j.cell.2021.12.032.

Hoffmann, M., Zhang, L., Kruger, N., Graichen, L., Kleine-Weber, H., Hofmann-Winkler, H., Kempf, A., Nessler, S., Riggert, J., Winkler, M.S., et al. (2021b). SARS-CoV-2 mutations acquired in mink reduce antibody-mediated neutralization. Cell Rep. *35*, 109017. https://doi.org/10.1016/j.celrep.2021.109017.

Hui, K.P.Y., Ho, J.C.W., Cheung, M.C., Ng, K.C., Ching, R.H.H., Lai, K.L., Kam, T.T., Gu, H., Sit, K.Y., Hsin, M.K.Y., et al. (2022). SARS-CoV-2 Omicron variant replication in human bronchus and lung ex vivo. Nature *603*, 715–720. https://doi.org/10.1038/s41586-022-04479-6.

Iketani, S., Liu, L., Guo, Y., Liu, L., Chan, J.F.W., Huang, Y., Wang, M., Luo, Y., Yu, J., Chu, H., et al. (2022). Antibody evasion properties of SARS-CoV-2 Omicron sublineages. Nature *604*, 553–556. https://doi.org/10.1038/s41586-022-04594-4.

Jones, B.E., Brown-Augsburger, P.L., Corbett, K.S., Westendorf, K., Davies, J., Cujec, T.P., Wiethoff, C.M., Blackbourne, J.L., Heinz, B.A., Foster, D., et al. (2021). The neutralizing antibody, LY-CoV555, protects against SARS-CoV-2 infection in nonhuman primates. Sci. Transl. Med. *13*. https://doi.org/10.1126/scitranslmed.abf1906.

Jung, C., Kmiec, D., Koepke, L., Zech, F., Jacob, T., Sparrer, K.M.J., and Kirchhoff, F. (2022). Omicron: what makes the latest SARS-CoV-2 variant of concern so concerning? J. Virol. *96*, jvi0207721. https://doi.org/10.1128/jvi.02077-21.

Karim, S.S.A., and Karim, Q.A. (2021). Omicron SARS-CoV-2 variant: a new chapter in the COVID-19 pandemic. Lancet *398*, 2126–2128. https://doi.org/10.1016/S0140-6736(21)02758-6.

Kim, C., Ryu, D.K., Lee, J., Kim, Y.I., Seo, J.M., Kim, Y.G., Jeong, J.H., Kim, M., Kim, J.I., Kim, P., et al. (2021). A therapeutic neutralizing antibody targeting receptor binding domain of SARS-CoV-2 spike protein. Nat. Commun. *12*, 288. https://doi.org/10.1038/s41467-020-20602-5.

Kleine-Weber, H., Elzayat, M.T., Wang, L., Graham, B.S., Muller, M.A., Drosten, C., Pohlmann, S., and Hoffmann, M. (2019). Mutations in the spike protein of Middle East respiratory syndrome coronavirus transmitted in korea increase resistance to antibody-mediated neutralization. J. Virol. *93*, e01381-18. https://doi.org/10.1128/JVI.01381-18.

Krammer, F. (2021). Correlates of protection from SARS-CoV-2 infection. Lancet *397*, 1421–1423. https://doi.org/10.1016/S0140-6736(21)00782-0.

Lumley, S.F., O'Donnell, D., Stoesser, N.E., Matthews, P.C., Howarth, A., Hatch, S.B., Marsden, B.D., Cox, S., James, T., Warren, F., et al. (2021). Antibody status and incidence of SARS-CoV-2 infection in health care workers. N. Engl. J. Med. *384*, 533–540. https://doi.org/10.1056/NEJMoa2034545.

Lyngse, F.P., Kirkeby, C.T., Denwood, M., Christiansen, L.E., Mølbak, K., Møller, C.H., Skov, R.L., Krause, T.G., Rasmussen, M., Sieber, R.N., et al. (2022). Transmission of SARS-CoV-2 omicron VOC subvariants BA.1 and BA.2: evidence from Danish households. Preprint at medRxiv. https://doi.org/10.1101/2022.01.28.22270044.

Mahase, E. (2022). Covid-19: what do we know about omicron sublineages? BMJ *376*, o358. https://doi.org/10.1136/bmj.o358.

McCallum, M., De Marco, A., Lempp, F.A., Tortorici, M.A., Pinto, D., Walls, A.C., Beltramello, M., Chen, A., Liu, Z., Zatta, F., et al. (2021). N-terminal domain antigenic mapping reveals a site of vulnerability for SARS-CoV-2. Cell *184*, 2332–2347.e16. https://doi.org/10.1016/j.cell.2021.03.028.

Meng, B., Abdullahi, A., Ferreira, I.A.T.M., Goonawardane, N., Saito, A., Kimura, I., Yamasoba, D., Gerber, P.P., Fatihi, S., Rathore, S., et al.; The CITIID-NIHR BioResource COVID-19 Collaboration; The Genotype to Phenotype Japan G2P-Japan Consortium; Ecuador-COVID19 Consortium (2022). Altered TMPRSS2 usage by SARS-CoV-2 Omicron impacts infectivity and fusogenicity. Nature *603*, 706–714. https://doi.org/10.1038/s41586-022-04474-x.

Piccoli, L., Park, Y.J., Tortorici, M.A., Czudnochowski, N., Walls, A.C., Beltramello, M., Silacci-Fregni, C., Pinto, D., Rosen, L.E., Bowen, J.E., et al. (2020). Mapping neutralizing and immunodominant sites on the SARS-CoV-2 spike receptor-binding domain by structure-guided high-resolution serology. Cell *183*, 1024–1042.e21. https://doi.org/10.1016/j.cell.2020.09.037.

Pinto, D., Park, Y.J., Beltramello, M., Walls, A.C., Tortorici, M.A., Bianchi, S., Jaconi, S., Culap, K., Zatta, F., De Marco, A., et al. (2020). Cross-neutralization of SARS-CoV-2 by a human monoclonal SARS-CoV antibody. Nature *583*, 290–295. https://doi.org/10.1038/s41586-020-2349-y.

Riepler, L., Rossler, A., Falch, A., Volland, A., Borena, W., von Laer, D., and Kimpel, J. (2020). Comparison of four SARS-CoV-2 neutralization assays. Vaccines (Basel) *9*, 13. https://doi.org/10.3390/vaccines9010013.

Rossler, A., Riepler, L., Bante, D., von Laer, D., and Kimpel, J. (2022). SARS-CoV-2 omicron variant neutralization in serum from vaccinated and convalescent persons. N. Engl. J. Med. *386*, 698–700. https://doi.org/10.1056/NEJMc2119236.

Saito, A., Irie, T., Suzuki, R., Maemura, T., Nasser, H., Uriu, K., Kosugi, Y., Shirakawa, K., Sadamasu, K., Kimura, I., et al.; The Genotype to Phenotype Japan G2P-Japan Consortium (2022). Enhanced fusogenicity and pathogenicity of SARS-CoV-2 Delta P681R mutation. Nature *602*, 300–306. https://doi.org/10.1038/s41586-021-04266-9.

Schmidt, F., Muecksch, F., Weisblum, Y., Da Silva, J., Bednarski, E., Cho, A., Wang, Z., Gaebler, C., Caskey, M., Nussenzweig, M.C., et al. (2022). Plasma neutralization of the SARS-CoV-2 omicron variant. N. Engl. J. Med. *386*, 599–601. https://doi.org/10.1056/NEJMc2119641.

Shi, R., Shan, C., Duan, X., Chen, Z., Liu, P., Song, J., Song, T., Bi, X., Han, C., Wu, L., et al. (2020). A human neutralizing antibody targets the

receptor-binding site of SARS-CoV-2. Nature *584*, 120–124. https://doi.org/10.1038/s41586-020-2381-y.

Suzuki, R., Yamasoba, D., Kimura, I., Wang, L., Kishimoto, M., Ito, J., Morioka, Y., Nao, N., Nasser, H., Uriu, K., et al.; The Genotype to Phenotype Japan G2P-Japan Consortium (2022). Attenuated fusogenicity and pathogenicity of SARS-CoV-2 Omicron variant. Nature *603*, 700–705. https://doi.org/10.1038/s41586-022-04462-1.

Takashita, E., Kinoshita, N., Yamayoshi, S., Sakai-Tagawa, Y., Fujisaki, S., Ito, M., Iwatsuki-Horimoto, K., Halfmann, P., Watanabe, S., Maeda, K., et al. (2022). Efficacy of antiviral agents against the SARS-CoV-2 omicron subvariant BA.2. N. Engl. J. Med. *386*, 1475–1477. https://doi.org/10.1056/NEJMc2201933.

VanBlargan, L.A., Errico, J.M., Halfmann, P.J., Zost, S.J., Crowe, J.E., Jr., Purcell, L.A., Kawaoka, Y., Corti, D., Fremont, D.H., and Diamond, M.S. (2022). An infectious SARS-CoV-2 B.1.1.529 Omicron virus escapes neutralization by therapeutic monoclonal antibodies. Nat. Med. *28*, 490–495. https://doi.org/10.1038/s41591-021-01678-y.

Weinreich, D.M., Sivapalasingam, S., Norton, T., Ali, S., Gao, H., Bhore, R., Musser, B.J., Soo, Y., Rofail, D., Im, J., et al. (2021). REGN-COV2, a neutralizing antibody cocktail, in outpatients with covid-19. N. Engl. J. Med. *384*, 238–251. https://doi.org/10.1056/NEJMoa2035002.

Xu, Z., Shi, L., Wang, Y., Zhang, J., Huang, L., Zhang, C., Liu, S., Zhao, P., Liu, H., Zhu, L., et al. (2020). Pathological findings of COVID-19 associated with acute respiratory distress syndrome. Lancet Respir. Med. *8*, 420–422. https://doi.org/10.1016/S2213-2600(20)30076-X.

Yu, J., Collier, A.r.Y., Rowe, M., Mardas, F., Ventura, J.D., Wan, H., Miller, J., Powers, O., Chung, B., Siamatu, M., et al. (2022). Neutralization of the SARS-CoV-2 omicron BA.1 and BA.2 variants. N. Engl. J. Med. *386*, 1579–1580. https://doi.org/10.1056/NEJMc2201849.

Zhang, L., Li, Q., Liang, Z., Li, T., Liu, S., Cui, Q., Nie, J., Wu, Q., Qu, X., Huang, W., and Wang, Y. (2022). The significant immune escape of pseudotyped SARS-CoV-2 variant Omicron. Emerg. Microbes Infect. *11*, 1–5. https://doi.org/10.1080/22221751.2021.2017757.

Zhao, H., Lu, L., Peng, Z., Chen, L.L., Meng, X., Zhang, C., Ip, J.D., Chan, W.M., Chu, A.W.H., Chan, K.H., et al. (2022). SARS-CoV-2 Omicron variant shows less efficient replication and fusion activity when compared with Delta variant in TMPRSS2-expressed cells. Emerg. Microbes Infect. *11*, 277–283. https://doi.org/10.1080/22221751.2021.2023329.

Zhou, P., Yang, X.L., Wang, X.G., Hu, B., Zhang, L., Zhang, W., Si, H.R., Zhu, Y., Li, B., Huang, C.L., et al. (2020). A pneumonia outbreak associated with a new coronavirus of probable bat origin. Nature *579*, 270–273. https://doi.org/10.1038/s41586-020-2012-7.

STAR★METHODS

KEY RESOURCES TABLE

REAGENT or RESOURCE	SOURCE	IDENTIFIER
Antibodies		
Casirivimab	laboratory of H.-M.J.	N/A
Imdevimab	laboratory of H.-M.J.	N/A
Bamlanivimab	laboratory of H.-M.J.	N/A
Etesevimab	laboratory of H.-M.J.	N/A
Cilgavimab	laboratory of H.-M.J.	N/A
Tixagevimab	laboratory of H.-M.J.	N/A
Regdanvimab	laboratory of H.-M.J.	N/A
Sotrovimab	laboratory of H.-M.J.	N/A
hIgG	laboratory of H.-M.J.	N/A
Recombinant anti-ACE2 Neutralizing Antibody	Sino Biological	Cat# 10108-MM37; RRID: N/A
Goat anti-Human IgG (H+L) Cross-Adsorbed Secondary Antibody, Alexa Fluor 488	Thermo Fisher Scientific	Cat# A-11013; RRID: AB_2534080
Anti-VSV-G antibody (I1, produced from CRL-2700 mouse hybridoma cells)	ATCC	Cat# CRL-2700; RRID: CVCL_G654
Bacterial and virus strains		
VSV*ΔG-FLuc	laboratory of Gert Zimmer	N/A
One Shot OmniMAX 2 T1R Chemically Competent *E. coli*	Thermo Fisher Scientific	Cat# C854003
Biological samples		
Vaccinee serum BNT/BNT/BNT (1)	laboratory of G.M.N.B.	N/A
Vaccinee serum BNT/BNT/BNT (2)	laboratory of G.M.N.B.	N/A
Vaccinee serum BNT/BNT/BNT (3)	laboratory of G.M.N.B.	N/A
Vaccinee serum BNT/BNT/BNT (4)	laboratory of G.M.N.B.	N/A
Vaccinee serum BNT/BNT/BNT (5)	laboratory of G.M.N.B.	N/A
Vaccinee serum BNT/BNT/BNT (6)	laboratory of G.M.N.B.	N/A
Vaccinee serum BNT/BNT/BNT (7)	laboratory of G.M.N.B.	N/A
Vaccinee serum BNT/BNT/BNT (8)	laboratory of G.M.N.B.	N/A
Vaccinee serum BNT/BNT/BNT (9)	laboratory of G.M.N.B.	N/A
Vaccinee serum BNT/BNT/BNT (10)	laboratory of G.M.N.B.	N/A
Vaccinee serum BNT/BNT/BNT (11)	laboratory of G.M.N.B.	N/A
Vaccinee serum BNT/BNT/BNT (12)	laboratory of G.M.N.B.	N/A
Vaccinee serum BNT/BNT/BNT (13)	laboratory of G.M.N.B.	N/A
Vaccinee serum BNT/BNT/BNT (14)	laboratory of G.M.N.B.	N/A
Vaccinee serum BNT/BNT/BNT (15)	laboratory of G.M.N.B.	N/A
Vaccinee serum AZ/AZ/BNT (01)	laboratory of G.M.N.B.	N/A
Vaccinee serum AZ/AZ/BNT (02)	laboratory of G.M.N.B.	N/A
Vaccinee serum AZ/AZ/BNT (03)	laboratory of G.M.N.B.	N/A
Vaccinee serum AZ/AZ/BNT (04)	laboratory of G.M.N.B.	N/A
Vaccinee serum AZ/AZ/BNT (05)	laboratory of G.M.N.B.	N/A
Vaccinee serum AZ/AZ/BNT (06)	laboratory of G.M.N.B.	N/A
Vaccinee serum AZ/AZ/BNT (07)	laboratory of G.M.N.B.	N/A
Vaccinee serum AZ/AZ/BNT (08)	laboratory of G.M.N.B.	N/A
Vaccinee serum AZ/AZ/BNT (09)	laboratory of G.M.N.B.	N/A
Vaccinee serum AZ/AZ/BNT (10)	laboratory of G.M.N.B.	N/A
Vaccinee serum AZ/AZ/BNT (11)	laboratory of G.M.N.B.	N/A

(*Continued on next page*)

Continued

REAGENT or RESOURCE	SOURCE	IDENTIFIER
Vaccinee serum AZ/AZ/BNT (12)	laboratory of G.M.N.B.	N/A
Vaccinee serum AZ/AZ/BNT (13)	laboratory of G.M.N.B.	N/A
Vaccinee serum AZ/AZ/BNT (14)	laboratory of G.M.N.B.	N/A
Vaccinee serum AZ/AZ/BNT (15)	laboratory of G.M.N.B.	N/A
Vaccinee serum AZ/BNT/BNT (01)	laboratory of G.M.N.B.	N/A
Vaccinee serum AZ/BNT/BNT (02)	laboratory of G.M.N.B.	N/A
Vaccinee serum AZ/BNT/BNT (03)	laboratory of G.M.N.B.	N/A
Vaccinee serum AZ/BNT/BNT (04)	laboratory of G.M.N.B.	N/A
Vaccinee serum AZ/BNT/BNT (05)	laboratory of G.M.N.B.	N/A
Vaccinee serum AZ/BNT/BNT (06)	laboratory of G.M.N.B.	N/A
Vaccinee serum AZ/BNT/BNT (07)	laboratory of G.M.N.B.	N/A
Vaccinee serum AZ/BNT/BNT (08)	laboratory of G.M.N.B.	N/A
Vaccinee serum AZ/BNT/BNT (09)	laboratory of G.M.N.B.	N/A
Vaccinee serum AZ/BNT/BNT (10)	laboratory of G.M.N.B.	N/A
Vaccinee serum AZ/BNT/BNT (11)	laboratory of G.M.N.B.	N/A
Vaccinee serum AZ/BNT/BNT (12)	laboratory of G.M.N.B.	N/A
Vaccinee serum AZ/BNT/BNT (13)	laboratory of G.M.N.B.	N/A
Vaccinee serum AZ/BNT/BNT (14)	laboratory of G.M.N.B.	N/A
Vaccinee serum AZ/BNT/BNT (15)	laboratory of G.M.N.B.	N/A
Chemicals, peptides, and recombinant proteins		
Soluble human ACE2 (sol-hACE2-Fc)	laboratory of S.P.	N/A
Critical commercial assays		
Beetle-Juice Kit	PJK	Cat# 102511
Gal-Screen β-Galactosidase Reporter Gene Assay System for Mammalian Cells	Thermo Fisher Scientific	Cat# T1027
GeneArt Gibson Assembly HiFi Master Mix	Thermo Fisher Scientific	Cat# A46627
Experimental models: Cell lines		
293T	DSMZ	Cat# ACC-635; RRID: CVCL_0063
A549-ACE2	laboratory of S.P.	N/A
BHK-21	laboratory of Georg Herrler	ATCC Cat# CCL-10; RRID: CVCL_1915
Caco-2	laboratory of S.P.	ATCC Cat# HTB-37; RRID: CVCL_0025
Calu-3	laboratory of Stephan Ludwig	ATCC Cat# HTB-55; RRID: CVCL_0609
Huh-7	laboratory of Thomas Pietschmann	JCRB Cat# JCRB0403; RRID: CVCL_0336
Vero	laboratory of Andrea Maisner	ATCC Cat# CRL-1587; RRID: CVCL_0603
Oligonucleotides		
pQCXIP F (GAGCTCGTTTAGTGAACCG)	Sigma-Aldrich	N/A
Omega (*Not*I) F (AAGGCCGCGGCCGCGCCA CCATGACCATGATTACGGATTCACTGG)	Sigma-Aldrich	N/A
Omega (*Pac*I) R (AAGGCCTTAATTAATTATTTT TGACACCAGACCAACTGG)	Sigma-Aldrich	N/A
Omega 754F (GCGGTGAAATTATCGATGAGC)	Sigma-Aldrich	N/A
Omega 1447F (TGGATGAAGACCAACCCTTCC)	Sigma-Aldrich	N/A
Omega 2173F (CATCGAGCTGGGTAATAAGC)	Sigma-Aldrich	N/A
Omega 3659F (TTACTGCGGCCTGTTTTGACC)	Sigma-Aldrich	N/A
SARS-2-S Seq-01 (CAAGATCTACAGCAAGCACACC)	Sigma-Aldrich	N/A

(*Continued on next page*)

Continued

REAGENT or RESOURCE	SOURCE	IDENTIFIER
SARS-2-S Seq-02 (GTCGGCGGCAACTACAATTAC)	Sigma-Aldrich	N/A
SARS-2-S Seq-03 (GCTGTCTGATCGGAGCCGAG)	Sigma-Aldrich	N/A
SARS-2-S Seq-04 (TGAGATGATCGCCCAGTACAC)	Sigma-Aldrich	N/A
SARS-2-S Seq-05 (GCCATCTGCCACGACGGCAAAG)	Sigma-Aldrich	N/A
pCG1 F (CCTGGGCAACGTGCTGGT)	Sigma-Aldrich	N/A
pCG1 R (GTCAGATGCTCAAGGGGCTTCA)	Sigma-Aldrich	N/A
Recombinant DNA		
SARS-2-SΔ18 (BA.2), codon-optimized, DNA strings	Thermo Fisher Scientific	N/A
SARS-2-SΔ18 (BA.3), codon-optimized, DNA strings	Thermo Fisher Scientific	N/A
Plasmid: pCG1	laboratory of Roberto Cattaneo	N/A
Plasmid: pCAGGS-VSV-G	laboratory of S.P.	N/A
Plasmid: pCG1-SARS-2-SΔ18 (B.1), codon-optimized	laboratory of S.P.	N/A
Plasmid: pCG1-SARS-2-SΔ18 (B.1.617.2), codon-optimized	laboratory of S.P.	N/A
Plasmid: pCG1-SARS-2-SΔ18 (B.1.1.529), codon-optimized	this study	N/A
Plasmid: pCG1-SARS-2-SΔ18 (BA.1), codon-optimized	laboratory of S.P.	N/A
Plasmid: pCG1-SARS-2-SΔ18 (BA.2), codon-optimized	this study	N/A
Plasmid: pCG1-SARS-2-SΔ18 (BA.3), codon-optimized	this study	N/A
Plasmid: pQCXIP_Human ACE2-cMYC	laboratory of S.P.	N/A
Plasmid: pQCXIP_Mouse ACE2-cMYC	laboratory of S.P.	N/A
Plasmid: pQCXIP_Bat (*Rhinolophus pearsonii*) ACE2-cMYC	laboratory of S.P.	N/A
Plasmid: pQCXIP_beta-galactosidase alpha fragment	this study	N/A
Plasmid: pQCXIP_beta-galactosidase omega fragment	this study	N/A
Plasmid: pCG1-solACE2-Fc	laboratory of S.P.	N/A
Software and algorithms		
Hidex Sense Microplate Reader Software	Hidex Deutschland Vertrieb GmbH	https://www.hidex.de
Adobe Photoshop CS5 Extended (version 12.0 × 32)	Adobe	https://www.adobe.com/
GraphPad Prism (version 8.3.0(538))	GraphPad Software	https://www.graphpad.com/
Flowing software (version 2.5.1)	Turku Bioscience	https://bioscience.fi/services/cell-imaging/flowing-software/
Microsoft Office Standard 2010 (version 14.0.7232.5000)	Microsoft Corporation	https://products.office.com/

RESOURCE AVAILABILITY

Lead contact

Further information and requests for resources and reagents should be directed to and will be fulfilled by the lead contact, Stefan Pöhlmann (spoehlmann@dpz.eu).

Materials availability

All materials and reagents will be made available upon installment of a material transfer agreement (MTA).

Data and code availability

- All data reported in this paper will be shared by the lead contact upon request.
- This paper does not report original code.
- Any additional information required for reanalyzing the data reported in this paper is available from the lead contact upon request

EXPERIMENTAL MODEL AND SUBJECT DETAILS

Cell cultures

293T (human, female, kidney; ACC-635, DSMZ; RRID: CVCL_0063), Vero (African green monkey, female, kidney; CRL-1587, ATCC; RRID: CVCL_0603, kindly provided by Andrea Maisner), Huh-7 cells (human, male, liver; JCRB Cat# JCRB0403; RRID: CVCL_0336,

kindly provided by Thomas Pietschmann), BHK-21 (Syrian hamster, male, kidney; CCL-10, ATCC; RRID: CVCL_1915, kindly provided by Georg Herrler) were maintained in Dulbecco's modified Eagle medium (DMEM, PAN-Biotech). Calu-3 (human, male, lung; HTB-55, ATCC; RRID: CVCL_0609, kindly provided by Stephan Ludwig) and Caco-2 cells (human, male, colon; HTB-37, ATCC, RRID: CVCL_0025) were maintained in minimum essential medium (GIBCO). A549-ACE2 (Hoffmann et al., 2021a), which were derived from parental A549 cells (human, male, lung; CRM-CCL-185, ATCC; RRID: CVCL_0023; kindly provided by Georg Herrler) were maintained in DMEM/F-12 medium (GIBCO). All media were supplemented with 10% fetal bovine serum (Biochrom) and 100 U/ml penicillin and 0.1 mg/ml streptomycin (PAA). Furthermore, Calu-3 and Caco-2 cells received 1× non-essential amino acid solution (from 100x stock, PAA) and 1 mM sodium pyruvate (GIBCO). All cell lines were incubated at 37°C in a humidified atmosphere containing 5% CO_2. Cell lines were validated by STR-typing, amplification and sequencing of a fragment of the cytochrome c oxidase gene, microscopic examination and/or according to their growth characteristics. In addition, cell lines were regularly tested for mycoplasma contamination. Transfection of cells was carried out by either calcium-phosphate precipitation, or using Lipofectamine 2000 or Lipofectamine LTX with Plus Reagent (both Thermo Fisher Scientific).

Human subjects

Sera from individuals vaccinated three times with BNT162b2 (BNT) (n = 15; seven males, eight females; median age 37 years, range: 27–60 years), two times with ChAdOx1-S (AZ) and one time with BNT (n = 15; five males, ten females; median age 42 years, range: 24–64 years), or one time with AZ and two times with BNT (n = 15; four males, eleven females; median age 37 years, range: 25–59 years) were collected median 21 days (range 14–83 days), 14 days (range 14–18 days) or 14 days (range 14–22 days), after receiving the last dose at Hannover Medical School (MHH). Sample collection was approved by the Institutional Review Board of MHH (8973_BO_K_2020) and specific details on the samples can be found in Table S3. To ensure that vaccinees were not (asymptomatically) infected before or during the vaccination period, sera were screened for the presence of antibodies specific to the SARS-CoV-2 S protein (before first vaccination) and nucleocapsid protein (after last vaccination). Serum samples were heat-inactivated at 56°C for 30 min prior to neutralization experiments.

METHODS DETAILS

Plasmids

Plasmids encoding VSV-G (vesicular stomatitis virus glycoprotein), SARS-CoV-2 S B.1 (codon optimized, contains C-terminal truncation of the last 18 amino acid), SARS-CoV-2 S B.1.617.2, SARS-CoV-2 S BA.1, soluble human ACE2 and ACE2 orthologues of human, mouse and horseshoe bat (Rhinolophus pearsonii) origin have been previously described (Arora et al., 2021; Brinkmann et al., 2017; Hoffmann et al., 2021a, 2022). For construction of expression plasmids for S proteins of SARS-CoV-2 variants BA.2 (GISAID Accession ID: EPI_ISL_8738174) and BA.3 (GISAID Accession ID: EPI_ISL_8801154) Gibson assembly was performed using five overlapping DNA strings for each S protein (Thermo Fisher Scientific), linearized (BamHI/XbaI digested) pCG1 plasmid and GeneArt Gibson Assembly HiFi Master Mix (Thermo Fisher Scientific). Gibson assembly was performed according to manufacturer's instructions. The pCG1 expression plasmid was kindly provided by Roberto Cattaneo, Mayo Clinic College of Medicine, Rochester, MN, USA. All S protein sequences and the underlying information (collection date, location) were obtained from the GISAID (global initiative on sharing all influenza data) database (https://www.gisaid.org/).

Expression plasmids for the quantitative cell-to-cell fusion assay were constructed as follows. To obtain the expression vector for the beta-galactosidase alpha fragment (MTDSLAVVLQRRDWENPGVTQLNRLAAHPPFASWRNSEEARTDRPSQQ, based on Burkard et al., 2014), a synthetic DNA fragment harboring the corresponding nucleotide fused to a C-terminal linker sequence (GSSGGGGSGGGGSSGGAQGNSV) and flanking restriction sites for cloning was ordered (Thermo Fisher Scientific). For generation of the expression vector for the beta-galactosidase omega fragment (GenBank: AUT10442.1) the respective sequence was PCR amplified from the pCAGGS-ΔM15 plasmid (Burkard et al., 2014) that was kindly provided by Berend Jan Bosch. Finally, the corresponding open reading frames were inserted into the pQCXIP plasmid making use of NotI and PacI restriction sites. The integrity of all sequences was analyzed using a commercial sequencing service (Microsynth SeqLab). Specific details on the cloning strategy and procedure can be attained upon request.

Production of soluble ACE2

The production of soluble human ACE2 C-terminally fused to the Fc-portion of human immunoglobulin G (solACE2-Fc) has been described in detail previously (Hoffmann et al., 2021b). Briefly, 293T cells were seeded and transfected with expression plasmid for soluble ACE2. After overnight incubation, the medium was replaced and the cells further incubated for 38 h before the supernatant was collected and centrifuged. Further, the clarified supernatant was concentrated (100×) using a Vivaspin protein concentrator column (molecular weight 30 kDa; Sartorius). The concentrated soluble ACE2 was aliquoted and stored at −80°C for further use.

Production of pseudotyped particles

Production of rhabdoviral pseudotypes bearing SARS-CoV-2 S protein has been previously described (Kleine-Weber et al., 2019). In brief, 293T cells were transfected with expression plasmid for SARS-CoV-2 S protein, VSV-G or empty plasmid (control) by calcium-phosphate precipitation. At 24 h posttransfection, cells were inoculated with VSV*ΔG-FLuc (Berger Rentsch and Zimmer, 2011), a replication-deficient vesicular stomatitis virus that lacks the genetic information for VSV-G and instead codes for two reporter

proteins, enhanced green fluorescent protein (eGFP) and firefly luciferase (FLuc) (kindly provided by Gert Zimmer) at an MOI of 3. Following 1 h of incubation, the inoculum was removed and cells were washed with phosphate-buffered saline (PBS). Subsequently, cells received culture medium containing anti-VSV-G antibody (culture supernatant from I1-hybridoma cells; ATCC no. CRL-2700; except for cells expressing VSV-G, which received only medium) in order to neutralize residual VSV*ΔG-FLuc transcomplemented with VSV-G. After 16–18 h, the culture supernatant was harvested, separated from cellular debris by centrifugation for 10 min at 4,000 × *g* at room temperature (RT), and the clarified supernatants were aliquoted and stored at −80°C.

Analysis of S-protein-mediated cell entry

For experiments assessing S protein-driven cell entry, target cells were seeded in 96-well plates and inoculated with equal volumes of pseudotype preparations. In case of experiments addressing S protein usage of different ACE2 orthologues as receptor, BHK-21 cells were transfected with the respective ACE2 expression plasmids or empty vector using Lipofectamine 2000 (Thermo Fisher Scientific) according to manufacturer's instructions. At 24 h post seeding (or transfection), the culture medium was removed and cells were inoculated with equal volumes of pseudotype preparations. In order to address the impact of antibody-mediated ACE2 blockade on S protein-driven cell entry, Vero cells were preincubated (30 min, 37°C) with medium containing different concentrations of anti-ACE2 neutralizing mouse monoclonal antibody (10108-MM37, Sino Biological), before equal volumes of pseudotype particles were added on top. Cells incubated with medium without antibody served as control (= 100 % cell entry). To investigate inhibition of S protein-driven cell entry by solACE2-Fc, pseudotype particles were preincubated (30 min, 37°C) with different dilutions of solACE2-Fc and subsequently inoculated onto Vero cells. Particles exposed to medium without soluble ACE2 served as control. To analyze neutralization of S protein-driven cell entry, pseudotype particles were pre-incubated (30 min at 37°C) with different concentrations (5, 0.5, 0.05, 0.005, 0.0005 μg/ml) of monoclonal antibody (casirivimab, imdevimab, bamlanivimab, etesevimab, cilgavimab, tixagevimab, regdanvimab, sotrovimab or an unrelated human control antibody) or combinations of these antibodies (casirivimab/imdevimab, bamlanivimab/etesevimab, cilgavimab/tixagevimab) or dilutions of vaccinee serum (1:50, 1:200, 1:800, 1:3,200, 1:12,800). Of note, for antibody cocktails each antibody was used at half the concentration in order to keep total antibody concentrations constant. Following incubation, mixtures were inoculated onto Vero cells with particles incubated only with medium serving as controls (0% inhibition).

In all cases, pseudotype entry efficiency was quantified by measuring the activity of virus-encoded luciferase at 16–18 h post inoculation. For this, cells were lysed using PBS containing 0.5% triton X-100 (Carl Roth) for 30 min at RT. Afterwards, cell lysates were transferred into white 96-well plates and mixed with luciferase substrate (Beetle- Juice, PJK) before luminescence was measured using a Hidex Sense Plate luminometer (Hidex).

Analysis of ACE2 binding by flow cytometry

In order to test binding of the different S proteins to ACE2, 293T cells were seeded in 6-well plates and transfected with expression plasmids for the respective SARS-CoV-2 S protein by calcium-phosphate precipitation. Cells transfected with empty plasmid served as a negative control. At 24 h posttransfection, the medium was replaced. At 48 h posttransfection, the culture medium was removed and cells were resuspended in PBS and transferred into 1.5 ml reaction tubes before being pelleted by centrifugation. All centrifugation steps were carried out at room temperature at 600 × *g* for 5 min. Subsequently, the supernatant was aspirated and the cells were washed with PBS containing 1 % bovine serum albumin (BSA, PBS-B) and pelleted by centrifugation. Next, the supernatant was removed and cell pellets were resuspended in 250 μl PBS-B containing soluble solACE2-Fc (1:100) and rotated for 60 min at 4°C using a Rotospin test tube rotator disk (IKA). Following incubation, cells were pelleted, resuspended in 250 μl PBS-B containing anti-human AlexaFlour-488-conjugated antibody (1:200; Thermo Fisher Scientific) and rotated again for 60 min at 4°C. Finally, the cells were washed with PBS-B, fixed by incubation in 1% paraformaldehyde solution for 30 min at RT, washed again and resuspended in 100 μl PBS-B before being subjected to flow cytometric analysis using an LSR II flow cytometer (BD Biosciences). Data were analyzed using the Flowing software (https://bioscience.fi/services/cell-imaging/flowing-software/) in order to determine the geometric mean channel fluorescence.

Qualitative cell-to-cell fusion assay

A549-ACE2 cells were grown in 12-well plates to reach ~75% confluency before being transfected with S protein expression plasmid or empty vector (control) using Lipofectamine LTX with Plus Reagent (Thermo Fisher Scientific) according to the manufacturer's instructions. At 24 h posttransfection, cells were fixed with 4% paraformaldehyde solution (30 min at room temperature), washed with PBS, air-dried and sequentially stained with May-Gruenwald and Giemsa solutions (each staining was performed for 30 min at room temperature). After each staining, cells were washed three times with deionized water and air-dried. Finally, S protein-driven cell-to-cell fusion was investigated by bright field microscopy using a Zeiss LSM800 confocal laser scanning microscope (Zeiss).

Quantitative cell-to-cell fusion assay

293T effector cells grown to ~75% confluency in 12-well plates were cotransfected with expression plasmids for the respective S protein or empty vector (1.5 μg/well) and the beta-galactosidase alpha fragment (0.5 μg/well) using Lipofectamine 2000 (Thermo Fisher Scientific) according to manufacturer's instructions. In addition, A549-ACE2 target cells grown to ~75% confluency in 96-well plates were transfected with expression vector for the beta-galactosidase omega fragment (0.2 μg/well) using Lipofectamine LTX with Plus Reagent (Thermo Fisher Scientific) according to the manufacturer's instructions. The culture medium was changed after

8 h. At 24 h posttransfection, effector cells were washed with PBS and resuspended in 450 μl culture medium, while the culture medium of the target cells was removed. Then, 100 μl effector cell suspension was added to the target cells in technical quadruplicates and cells were incubated for additional 24 h. Next, beta-galactosidase substrate (Gal-Screen, Thermo Fisher Scientific) was added (100 μl/well) and samples were incubated for 90 min in the dark at room temperature before luminescence was recorded using a Hidex Sense plate luminometer (Hidex).

QUANTIFICATION AND STATISTICAL ANALYSIS

The results on S protein-driven cell entry represent average (mean) data acquired from six to twelve biological replicates, each conducted with four technical replicates. Transduction was normalized against that measured for SARS-CoV-2 S B.1 (set as 1). Alternatively, transduction was normalized against the background signal (luminescence measured for cells inoculated with particles bearing no viral glycoprotein; set as 1). For ACE2 binding analyzed by flow cytometry, the average (mean) geometric mean channel fluorescence from six biological replicates is presented, each conducted with single samples. For blockade of S protein-driven cell entry by an anti-ACE2 antibody, the average (mean) data of three biological replicates are presented, each performed with four technical replicates where S-protein-driven cell entry was analyzed and normalized to samples without anti-ACE2 (set as 1). For blockade of S protein-driven cell entry by solACE2-Fc, the average (mean) data of three biological replicates are presented, each performed with four technical replicates, where S-protein-driven cell entry was analyzed and normalized to samples without solACE2-Fc (= 0% inhibition). For experiments investigating usage of different ACE2 orthologues, the average (mean) data of three biological replicates are presented, each performed with four technical replicates, where cell entry of pseudovirus particles was analyzed and normalized to particles bearing no viral glycoprotein (set as 1). The data of the qualitative fusion assay show representative images from three biological replicates, each performed with single samples. For the quantitative cell-cell fusion assay, the average (mean) data of three biological replicates are presented, each performed with four technical replicates. The results on neutralization of S-protein-driven cell entry by monoclonal antibodies represent average (mean) data from three biological replicates each performed with four technical replicates. Transduction was normalized to samples without antibody (= 0% inhibition). The results on neutralization of S protein-driven cell entry by vaccinee sera represent average (mean) data from a single biological replicate performed with four technical replicates. Transduction was normalized to samples without serum (= 0% inhibition).

The inhibitory concentration 50 (IC50) values for the monoclonal antibodies and neutralization titer 50 (NT50) values for vaccinee sera were calculated by a non-linear regression model with variable slope. Error bars show either the standard deviation (SD), the standard error of the mean (SEM) or the 95% confidence intervals. Data were analyzed using Microsoft Excel (as part of the Microsoft Office software package, version 2019, Microsoft Corporation) and GraphPad Prism 8 version 8.4.3 (GraphPad Software). Statistical significance was analyzed by two-tailed Student's t test with Welch correction (pseudotype entry, ACE2 binding, quantitative cell-to-cell fusion assay), two-way analysis of variance with Dunnett's post hoc tests (blockade of S protein-driven cell entry by anti-ACE2 antibody, solACE2-Fc or therapeutic antibodies) or two-tailed Mann-Whitney test (neutralization by vaccinee sera). Only p values of 0.05 or lower were considered statistically significant ($p > 0.05$, not significant [ns]; $p \leq 0.05$, *; $p \leq 0.01$, **; $p \leq 0.001$, ***). Details on the statistical test and the error bars can be found in the figure legends.